Phase transitions in coupled map lattices and in associated probabilistic cellular automata

Wolfram Just*
School of Mathematical Sciences, Queen Mary, University of London, Mile End Road, London E1 4NS, United Kingdom
(Received 12 May 2006; revised manuscript received 17 July 2006; published 12 October 2006)

Analytical tools are applied to investigate piecewise linear coupled map lattices in terms of probabilistic cellular automata. The so-called disorder condition of probabilistic cellular automata is closely related with attracting sets in coupled map lattices. The importance of this condition for the suppression of phase transitions is illustrated by spatially one-dimensional systems. Invariant densities and temporal correlations are calculated explicitly. Ising type phase transitions are found for one-dimensional coupled map lattices acting on repelling sets and for a spatially two-dimensional Miller-Huse-like system with stable long time dynamics. Critical exponents are calculated within a finite size scaling approach. The relevance of detailed balance of the resulting probabilistic cellular automaton for the critical behavior is pointed out.

DOI: 10.1103/PhysRevE.74.046209 PACS number(s): 05.45.Ra, 05.10.−a, 05.70.Fh

I. INTRODUCTION

Nonlinear and chaotic behavior in dynamical systems with a small or finite number of degrees of freedom is nowadays a very well-established topic [1,2]. Features of chaotic dynamics can be observed in diverse real world experiments [3] and can be captured by quite abstract mathematical models even quantitatively [4], owing to universal properties and structural stability. The situation is less complete when the dynamics of systems with a large number of degrees of freedom is at stake when not close to thermodynamic equilibrium. Of course, over the past decades there has been made substantial progress in particular fields such as, e.g., nonequilibrium pattern formation where well-established approaches are available in the literature [5]. In addition, paradigmatic model systems have been developed as well, e.g., for the dynamics of interacting oscillators in random environments [6]. But there is still no comprehensive picture when interacting chaotic subunits are considered. Models of coupled maps which have been proposed decades ago and which have been investigated extensively by numerical means [7,8] have turned out to be extremely difficult to treat in a rigorous manner [9–12]. Furthermore, the relation between coupled map lattices and real experimental phenomena is not obvious. But such a shortcoming also appears when low-dimensional chaotic behavior is studied in terms of maps. On the other hand, coupled map lattices are a quite promising class of dynamical systems since mathematical tools such as symbolic dynamics link coupled map lattices with the statistical mechanics of spin systems [2,13]. Depending on the implementation one either ends up with an equilibrium spin model where the Hamiltonian typically has quite intricate interactions [9,10] or with a dynamical spin model where the time evolution requires simultaneous updates of the lattice sites [14]. The latter class of systems, usually called probabilistic cellular automata, is quite well established in mathematical statistical physics [15,16]. Last, but not least, numerical simulations of coupled map lattices show phase transition like behavior in the limit of a large system size [17,18]. Thus, despite that there is no direct link to experimental phenomena, coupled map lattices are interesting in their own right as they constitute a quite rich model class for nonequilibrium statistical physics.

Here we will recall the relation between certain types of simple piecewise linear coupled map lattices and the corresponding description in terms of the statistical mechanics of spin models. As already pointed out it has been suggested that qualitative changes of the dynamics of coupled map lattices in the limit of a large system size can be understood in terms of equilibrium phase transitions in spin models [9], although it is quite subtle to give the notion of a phase transition in dynamical systems a proper meaning [19]. Here, however, we skip these subtleties and we illustrate such a concept with quite simple piecewise linear map lattices only. Actually, it will be shown in Sec. III that dynamical systems with attracting and repelling invariant sets may behave substantially different with respect to the occurrence of phase transitions since the first type of dynamical systems yields severe constraints for the resulting spin Hamiltonian. Thus, while spatially one-dimensional expanding coupled map lattices with repelling invariant sets display Ising phase transitions [20] such transitions are less likely to occur in one-dimensional dynamical systems with chaotic attractors. In fact, a similar feature is quite well known in the context of probabilistic cellular automata [15,16]. Phase transitions which occur in spatially one-dimensional coupled map lattices with absorbing states (cf. [21], and references theirin) seem to be somehow suppressed for expanding coupled map lattices. Therefore, we focus in Sec. IV on a spatially two-dimensional model. Within such a setup numerical simulations indicated that Ising-like phase transitions may occur [17]. But careful analysis of the numerical data showed slight deviations from the Ising universality class [22]. Such deviations have been attributed to the temporal evolution in coupled map lattices which require a simultaneous update of lattice sites, in contrast to standard algorithms for simulating the statistical mechanics of equilibrium spin models which rely on some version of random or sequential updates [23,24]. We are going to introduce a piecewise linear spatially two-dimensional coupled map lattice which shares the essential features of the Miller-Huse model but which can be dealt with analytically by the methods introduced previously.

*Electronic address: w.just@qmul.ac.uk

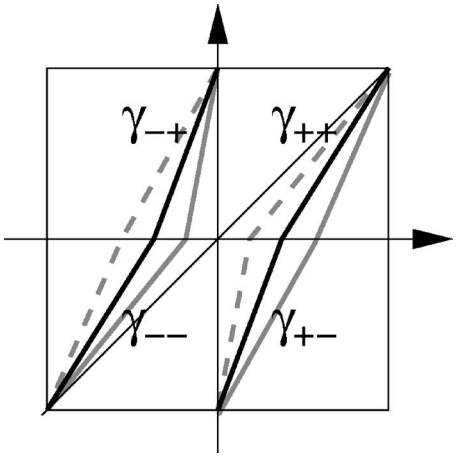

FIG. 1. Piecewise linear symmetric expanding Markov map (solid line). The derivative of the map on the cylinder set $U_{\sigma\tau}$ is denoted by $\gamma_{\sigma\tau}$, $\sigma,\tau\in\{-1,1\}$. Explicit time-dependent modulations of the map are indicated in gray [cf. Eq. (1)].

Actually, we will point out that detailed balance of the corresponding probabilistic cellular automaton may play a crucial role for the critical behavior. Several critical exponents will be determined by finite size scaling methods in Sec. V.

Some considerations of the subsequent sections are quite well established in the literature, in particular, the basic remarks of Sec. II and the considerations contained in the appendices. But to keep our presentation self-contained and accessible for a nonspecialized audience the concepts will be introduced from scratch in an elementary way. As a byproduct we are able to introduce the necessary notation.

II. PRELIMINARY REMARKS ON SYMBOLIC DYNAMICS

To begin with we first recall some very basic facts about piecewise linear Markov maps [2] and of the construction of coupled map lattices which can be solved analytically through symbolic dynamics. For the purpose of illustration consider the one-dimensional map $x_{n+1}=f(x_n)$ defined on $[-1,1]$ which is depicted in Fig. 1. Although our considerations will work for asymmetric cases as well we will restrict our considerations mainly to inversion symmetric maps. The map admits two invertible branches $f_\pm$ on $[-1,0]$ and $[0,1]$, respectively. The corresponding preimages of the domain, $U_\sigma=f_\sigma^{-1}[-1,1]$, $\sigma\in\{-1,1\}$, yield a generating partition since we are considering expanding maps, i.e., maps with slopes larger than one. For any fixed symbol sequence $(\sigma_0,\sigma_1,\sigma_2,\ldots,)$ the so-called cylinder sets $U_{\sigma_0,\ldots,\sigma_n}=(f_{\sigma_0}^{-1}\circ f_{\sigma_1}^{-1}\cdots\circ f_{\sigma_n}^{-1})[-1,1]$ yield a sequence of nested intervals. Since the length of these intervals decrease exponentially due to the expansiveness of the map, $|f'(x)|>1$, such a sequence finally singles out a phase space point $x_{\sigma_0,\sigma_1,\ldots,}$ where by construction the itinerary of this point is determined by the infinite symbol sequence. In order to ensure for simple statistical properties of the dynamics we will assume that the map acts linear on the cylinder sets of the second generation, i.e., on U_{σ_0,σ_1}, and we denote the modulus of the slope by $\gamma_{\sigma_0,\sigma_1}$. Thus, the whole dynamics is mapped to a symbol shift of infinite symbol sequences $(\sigma_0,\sigma_1,\sigma_2,\ldots,)$. Actually, the current map has much in common with the statistical mechanics of the nearest neighbor coupled Ising chain [25].

It is worth mentioning that the whole construction of the symbolic dynamics works in the same way if the map depends explicitly on the time n, as long as it still falls within the class of piecewise linear Markov maps. Thus, the time-dependent modulation indicated in Fig. 1 with time-dependent slopes still allows for the same symbolic description. Such an observation is the main clue to construct a coupled map lattice based on piecewise linear Markov maps.

The piecewise linear expanding Markov map is the starting point to introduce a spatially one-dimensional coupled map lattice. Let ν, $0\leqslant\nu\leqslant L-1$, denote the lattice sites, $\underline{x}=(x^{(0)},x^{(1)},\ldots,x^{(L-1)})$ the actual state of the system, and $\underline{\sigma}=(\sigma^{(0)},\sigma^{(1)},\ldots,\sigma^{(L-1)})$ the symbolic state where $\sigma^{(\nu)}=\mathrm{sgn}(x^{(\nu)})$. As far as the spatial coupling is concerned we will restrict ourselves to a simple case, i.e. a unidirectional nearest neighbor coupling. However, the subsequent consideration may be applied to more general situations as well. Finally, periodic boundary conditions will be imposed.

On each lattice site ν a map depicted in Fig. 1 acts on the coordinate $x_n^{(\nu)}$. The values of the local slope depend on the sign of the right nearest neighbor, i.e., on $\sigma_n^{(\nu+1)}$. Thus the dynamics is given by

$$x_{n+1}^{(\nu)}=f(x_n^{(\nu)};\sigma_n^{(\nu+1)}):=\begin{cases}-1+\gamma_{--}[\sigma_n^{(\nu+1)}](x_n^{(\nu)}+1) & \text{if} \quad -1\leqslant x_n^{(\nu)}<-1+1/\gamma_{--}[\sigma_n^{(\nu+1)}]\\ 1+\gamma_{-+}[\sigma_n^{(\nu+1)}]x_n^{(\nu)} & \text{if} \quad -1/\gamma_{-+}[\sigma_n^{(\nu+1)}]\leqslant x_n^{(\nu)}<0\\ -1+\gamma_{+-}[\sigma_n^{(\nu+1)}]x_n^{(\nu)} & \text{if} \quad 0<x_n^{(\nu)}\leqslant 1/\gamma_{+-}[\sigma_n^{(\nu+1)}]\\ 1+\gamma_{++}[\sigma_n^{(\nu+1)}](x_n^{(\nu)}-1) & \text{if} \quad 1-1/\gamma_{++}[\sigma_n^{(\nu+1)}]<x_n^{(\nu)}\leqslant 1\end{cases}. \tag{1}$$

The spatial coupling is mediated by the symbolic coordinate $\sigma_n^{(\nu+1)}$ only. Thus Eq. (1) has much in common with a skew product structure. Such a special type of coupling enables us to provide a full analytical solution, although the usually considered diffusive coupling is not covered by such a construction.

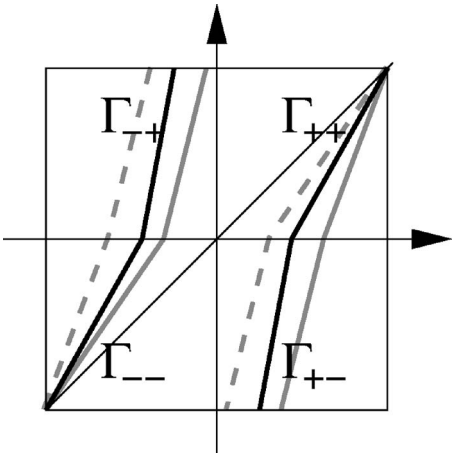

FIG. 2. Piecewise linear expanding Markov map with repelling invariant set. The value of the derivative is indicated by $\Gamma_{\sigma\tau}$, $\sigma,\tau \in \{-1,1\}$. Explicit time-dependent modulations of the map are displayed in gray. (cf. Fig. 1).

The values of the slopes $\gamma_{\tau\sigma}[\tilde{\tau}]$ are the parameters of the coupled map lattice determined by Eq. (1). Since we are considering a map with an attracting set we have to impose the constraint

$$\frac{1}{\gamma_{--}[\sigma]} + \frac{1}{\gamma_{-+}[\sigma]} = \frac{1}{\gamma_{+-}[\sigma]} + \frac{1}{\gamma_{++}[\sigma]} = 1. \tag{2}$$

If we confine for simplicity to the setup of inversion symmetric systems the slopes may be expressed in terms of the symbols $\sigma^{(\nu)}, \tau^{(\nu)} \in \{-1,1\}$ by

$$\gamma_{\tau^{(\nu)}\sigma^{(\nu)}}[\tau^{(\nu+1)}] = \exp(-\lambda\sigma^{(\nu)}\tau^{(\nu)} - \mu\sigma^{(\nu)}\tau^{(\nu+1)} - \alpha\tau^{(\nu)}\tau^{(\nu+1)} - \beta), \tag{3}$$

where the last two contributions in the exponent take care of the normalization (2). Thus

$$1 = 2\cosh(\lambda+\mu)\exp(\alpha+\beta),$$
$$1 = 2\cosh(\lambda-\mu)\exp(-\alpha+\beta) \tag{4}$$

holds and only two of the four parameters λ, μ, α, β can be chosen independently.

The symbolic dynamics of the coupled map lattice (1) is constructed in precisely the same way as for the single site map. Given a semi-infinite symbol lattice $(\underline{\sigma}_0, \underline{\sigma}_1, \ldots,)$ one obtains through the inverse branches of the map lattice a sequence of nested L-dimensional cubes which single out a phase space point $\underline{x}_{\underline{\sigma}_0,\underline{\sigma}_1,\ldots,}$. The itinerary of this point when applying Eq. (1) is given by the symbol lattice.

The restriction imposed by the condition (2) on the slopes will turn out to be quite severe. We, therefore, recall a second coupled map lattice without such a constraint [20]. But we have to pay the price that the invariant set is no longer an attractor. The type of single site maps are displayed in Fig. 2. Constructing the cylinder sets through the inverse branches we clearly obtain the recursive construction of a Cantor set. Phase space points not contained in this set will leave the domain on iteration. For the slopes itself we may allow for a time-dependent modulation which is caused again by the symbol of the right nearest neighbor when placing these maps on a one-dimensional lattice. Thus, the dynamical system reads

$$x_{n+1}^{(\nu)} = F(x_n^{(\nu)}; \sigma_n^{(\nu+1)}), \tag{5}$$

where the analytical expression for the right-hand side is essentially given by Eq. (1) when replacing $\gamma_{\tau\sigma}[\tilde{\tau}]$ by $\Gamma_{\tau\sigma}[\tilde{\tau}]$. For the choice of the local slopes $\Gamma_{\tau\sigma}[\tilde{\tau}]$ we have more freedom since nothing like the normalization (2) has to be applied. Later on we will adopt the expression

$$\Gamma_{\tau^{(\nu)}\sigma^{(\nu)}}[\tau^{(\nu+1)}] = \exp(-J\sigma^{(\nu)}\tau^{(\nu)} - J\tau^{(\nu)}\tau^{(\nu+1)} - E_0) \tag{6}$$

with constants J and E_0. This particular choice links the statistical properties of the coupled map lattice (5) with the two-dimensional Ising model. However, from the topological point of view there is not much difference between the models (1) and (5) since the symbolic dynamics is constructed essentially in the same way.

III. ANALYSIS OF THE PROBABILISTIC CELLULAR AUTOMATA

Since the models (1) and (5) allow for an explicit construction of the symbolic dynamics and since the simple topological structure nicely complies with the piecewise linear structure we can write down the time evolution of the probability distribution quite straightforwardly [14]. Let us first consider the map lattice (1). If $p_n(\underline{\sigma})$ denotes the probability to find the phase space point in hypercube $U_{\underline{\sigma}}$ at time n then the time evolution is governed by a master equation (cf. Appendix A for details)

$$p_{n+1}(\underline{\sigma}) = \sum_{\underline{\tau}} W_f(\underline{\sigma};\underline{\tau}) p_n(\underline{\tau}). \tag{7}$$

The transition rates $W_f(\underline{\sigma};\underline{\tau})$ appearing in Eq. (7) are obtained by comparison with Eq. (A4) to be the Jacobian of the map lattice (1). Taking Eq. (3) into account we obtain

$$W_f(\underline{\sigma};\underline{\tau}) = \prod_{\nu} \frac{1}{\gamma_{\tau^{(\nu)}\sigma^{(\nu)}}[\tau^{(\nu+1)}]} = \exp\left[\sum_{\nu} (\sigma^{(\nu)} H_\nu(\underline{\tau}) + \alpha\tau^{(\nu)}\tau^{(\nu+1)} + \beta)\right], \tag{8}$$

where a local field has been introduced by the abbreviation

$$H_\nu(\underline{\tau}) = \lambda\tau^{(\nu)} + \mu\tau^{(\nu+1)}. \tag{9}$$

The different parameters appearing in the transition rate (8) are related to each other by Eq. (4) since we are considering a system with an attracting set. The corresponding condition (2) ensures the normalization

$$\sum_{\underline{\sigma}} W_f(\underline{\sigma};\underline{\tau}) = 1 \tag{10}$$

which guarantees that the probabilities appearing in Eq. (7) remain normalized. Equation (7) describes transitions between states of a spin chain $\underline{\sigma}$ with synchronous updates at

the individual sites. Such a model is usually called a probabilistic cellular automaton contrary to the widely known kinetic Ising models [23] where updates are usually performed on a random or sequential basis. It is quite well established that detailed balance in probabilistic cellular automata requires a local field which is symmetric with respect to lattice sites (cf. e.g., [15,26]). Thus, in view of Eq. (9) detailed balance is violated. Such a property is, of course, not surprising as unidirectional coupling gives rise to a trivial transport mechanism. Because of the lack of detailed balance the computation of the stationary density $p_*(\underline{\sigma})$ may already pose a challenge, not to mention temporal correlations and eigenvalue spectra of the transition matrix. Here we will recall that the model defined by Eqs. (8) and (9) admits a complete analytical solution (cf. [15] and Appendix B).

The key for the determination of the stationary density is the normalization (2) which is essentially the reason for the conservation of probability, Eq. (10). In view of Eq. (3) the normalization reads

$$1 = \sum_{\sigma^{(\nu)}} \exp(\lambda \sigma^{(\nu)} \tau^{(\nu)} + \mu \sigma^{(\nu)} \tau^{(\nu+1)}) \exp(\alpha \tau^{(\nu)} \tau^{(\nu+1)} + \beta). \tag{11}$$

Then straightforward computation yields

$$\sum_{\underline{\tau}} W_f(\underline{\sigma};\underline{\tau}) \prod_{\nu} \exp(-\alpha \tau^{(\nu)} \tau^{(\nu+1)} - \beta) = \sum_{\underline{\tau}} \prod_{\nu} \exp(\lambda \tau^{(\nu)} \sigma^{(\nu)} + \mu \tau^{(\nu)} \sigma^{(\nu-1)}) = \prod_{\nu} \exp(-\alpha \sigma^{(\nu)} \sigma^{(\nu-1)} - \beta). \tag{12}$$

Thus, thanks to the nearest neighbor coupling in the local field (9) the stationary distribution is given by

$$p_*(\underline{\sigma}) = \frac{1}{Z} \exp\left(-\alpha \sum_{\nu} \sigma^{(\nu)} \sigma^{(\nu+1)}\right), \tag{13}$$

where Z is determined by normalization. The stationary distribution coincides with the canonical distribution of a nearest neighbor coupled Ising chain although the dynamics of the probabilistic cellular automaton does not fulfill detailed balance. Such a feature is also known from kinetic Ising models which can be derived from the current coupled map lattice when a perturbation expansion in terms of spin flip processes is applied [27].

As for the dynamics of the model (7) we will solve the eigenvalue equation of the transition matrix. For that purpose let us introduce the abbreviation

$$s_\nu(\underline{\sigma}) = \sigma^{(\nu)} p_*(\underline{\sigma}). \tag{14}$$

A computation quite similar to Eq. (12) yields

$$\sum_{\underline{\tau}} W_f(\underline{\sigma};\underline{\tau}) s_\nu(\underline{\tau}) = \frac{1}{Z} \sum_{\underline{\tau}} \left(\prod_{\rho(\neq\nu)} \exp(\lambda \tau^{(\rho)} \sigma^{(\rho)} + \mu \tau^{(\rho)} \sigma^{(\rho-1)} + \beta) \right) \tau^{(\nu)} \exp(\lambda \tau^{(\nu)} \sigma^{(\nu)} + \mu \tau^{(\nu)} \sigma^{(\nu-1)} + \beta) = \frac{1}{Z} \left(\prod_{\rho} \sum_{\tau^{(\rho)}} \exp(\lambda \tau^{(\rho)} \sigma^{(\rho)} + \mu \tau^{(\rho)} \sigma^{(\rho-1)} + \beta) \right) \frac{\sum_{\tau^{(\nu)}} \tau^{(\nu)} \exp(\lambda \tau^{(\nu)} \sigma^{(\nu)} + \mu \tau^{(\nu)} \sigma^{(\nu-1)} + \beta)}{\sum_{\tau^{(\nu)}} \exp(\lambda \tau^{(\nu)} \sigma^{(\nu)} + \mu \tau^{(\nu)} \sigma^{(\nu-1)} + \beta)} = p_*(\underline{\sigma}) \tanh(\lambda \sigma^{(\nu)} + \mu \sigma^{(\nu-1)}) = \tfrac{1}{2}[s_\nu(\underline{\sigma}) + s_{\nu-1}(\underline{\sigma})] \tanh(\lambda + \mu) + \tfrac{1}{2}[s_\nu(\underline{\sigma}) - s_{\nu-1}(\underline{\sigma})] \tanh(\lambda - \mu). \tag{15}$$

Therefore the function (14) yields an invariant subspace of the transition matrix with the simple recurrence rule (15). The corresponding eigenvalue problem can be solved by Fourier transformation in a straightforward way. We thus obtain for the eigenvalues

$$\Lambda_q = \frac{\tanh(\lambda + \mu) + \tanh(\lambda - \mu)}{2} + \exp(iq) \frac{\tanh(\lambda + \mu) - \tanh(\lambda - \mu)}{2} \tag{16}$$

and for the eigenvectors

$$r_q(\underline{\sigma}) = \sum_{\nu} \exp(iq\nu) s_\nu(\underline{\sigma}) = \sum_{\nu} \sigma^{(\nu)} \exp(iq\nu) p_*(\underline{\sigma}), \tag{17}$$

where the values of the wave number are fixed by periodic boundary condition $q = 2\pi\ell/L$, $0 \leq \ell \leq L-1$. The imaginary part of the spectrum (16) reflects the transport in the system induced by the unidirectional coupling. The modulus of the eigenvalues (16) is smaller than one indicating an exponential decay of the pair correlation function and an exponential decay of the transient dynamics. Thus, no phase transition is expected to occur for our model. A similar reasoning may be applied to compute the other eigenvalues governing the decay of higher order correlation functions.

Given the Markovian property of the evolution equation (7) the probability of finding a finite time series of states $(\underline{\sigma}_0, \underline{\sigma}_1, \ldots, \underline{\sigma}_n)$ is essentially determined by the product of the transition rates, i.e., by

$$W_f(\underline{\sigma}_n;\underline{\sigma}_{n-1}) \ldots W_f(\underline{\sigma}_1;\underline{\sigma}_0) = \exp\left(\sum_{\nu} \sum_{k} (\lambda \sigma_{k+1}^{(\nu)} \sigma_k^{(\nu)} + \mu \sigma_{k+1}^{(\nu)} \sigma_k^{(\nu+1)} + \alpha \sigma_k^{(\nu)} \sigma_k^{(\nu+1)} + \beta) \right). \tag{18}$$

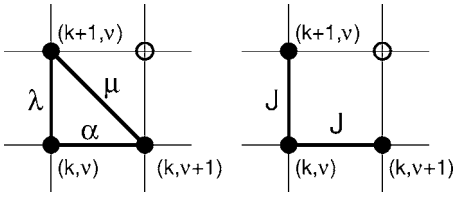

FIG. 3. Diagrammatic view of the interactions in the two-dimensional Ising Hamiltonians Eq. (18) (left) and Eq. (20) (right).

Obviously, such a probability can be cast into the form of a canonical weight of a two-dimensional Ising lattice $(\underline{\sigma}_0, \underline{\sigma}_1, \ldots, \underline{\sigma}_n)$ with nearest neighbor and diagonal coupling (cf. Fig. 3). Actually, the transition matrix of the probabilistic cellular automaton (7) is just the transfer matrix of this two-dimensional Ising Hamiltonian. Because of the normalization (4) the coupling coefficients λ, μ, α cannot be chosen independently. As we have just shown such a constraint prevents a phase transition from taking place in the thermodynamic limit. Such limitations are quite well established in the context of probabilistic cellular automata [15,16] and the constraints are called for historical reasons "disorder conditions."

The situation is quite different for coupled repeller maps where the disorder condition can be avoided. Although the dynamics of the probabilities is again governed by a master equation with transition probabilities being determined by the Jacobian of the map lattice

$$W_F(\underline{\sigma};\underline{\tau}) = \prod_{\nu} \frac{1}{\Gamma_{\tau^{(\nu)}\sigma^{(\nu)}}[\tau^{(\nu+1)}]} \tag{19}$$

and the probability for finding a symbol sequence $(\underline{\sigma}_0, \underline{\sigma}_1, \ldots, \underline{\sigma}_n)$ is essentially determined by

$$W_F(\underline{\sigma}_n;\underline{\sigma}_{n-1}) \ldots W_F(\underline{\sigma}_1;\underline{\sigma}_0) = \exp\left(\sum_{\nu}\sum_{k} (J\sigma_{k+1}^{(\nu)}\sigma_k^{(\nu)} + J\sigma_k^{(\nu)}\sigma_k^{(\nu+1)} + E_0)\right) \tag{20}$$

we now obtain by construction the canonical weight of the nearest neighbor coupled two-dimensional Ising model. In such a case a phase transition occurs for sufficiently large coupling strength J which is reflected by the spectral structure of the corresponding transfer matrix $W_F(\underline{\sigma};\underline{\tau})$ [28]. Details of the analysis of the corresponding coupled map lattice have been already published recently [20]. While the phase transition of our first model was prohibited by the constraints imposed by the attracting set the absence of such a constraint for the repeller system allows for the occurrence of different ergodic components in the thermodynamic limit.

IV. ANALYTICAL SOLUTION OF A MILLER-HUSE-TYPE MAP LATTICE

Phase transitions in spatially one-dimensional probabilistic cellular automata may be inhibited by constraints imposed by attracting sets as shown in the previous section. But such transitions, in particular, Ising-type phase transitions, occur when repelling states are allowed as well. The phase transition has been related to spatiotemporal symbolic patterns in order to generate equivalent two-dimensional spin Hamiltonians with short range interactions. The plain spatial correlations of such models, e.g., the stationary density of the probabilistic cellular automaton displays phase transition behavior as well. Of course, $\ln p_*(\underline{\sigma})$ yields only a one-dimensional spin Hamiltonian. But the stationary density which is just an eigenstate of the transition matrix $W(\underline{\sigma};\underline{\tau})$ contains quite nontrivial long range spin interactions (cf. e.g., [28] for the eigenvector of the Ising transfer matrix) reflecting the occurrence of the phase transition. Thus, an alternative for investigating phase transition behavior of coupled map lattices and of the corresponding probabilistic cellular automata consists in the investigation of the stationary density. Whenever detailed balance is obeyed and when the transition rates are local then we suspect that the corresponding stationary density yields a Hamiltonian with short range interactions only (cf. Appendix B). In such a context phase transitions can only occur when we study spatially two-dimensional lattices. In what follows we will recall the famous Miller-Huse model and its critical behavior in view of these statements.

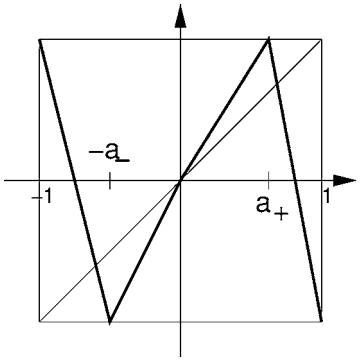

FIG. 4. Single site map of the coupled map lattice defined by Eq. (21).

More than a decade ago a spatially two-dimensional coupled map lattice was introduced which mimics to some extent a two-dimensional Ising model [17]. The single site map consisted of a kind of antisymmetric tent map (cf. Fig. 4) while for the spatial coupling the usual nearest neighbor diffusive coupling was employed which is frequently used in numerical studies of coupled map lattices. Simulations showed an Ising-like phase transition. Subsequent careful studies based on finite size scaling indicated that there are deviations in some critical exponents such that the coupled map lattice does not belong to the Ising universality class [22]. The behavior has been suggested to be related with the simultaneous updating procedure taking place in coupled map lattices contrary to random or sequential updates applied in kinetic Ising models.

In order to address this kind of problem in analytical terms let us introduce a variant of the Miller-Huse model which can be dealt with in an analytical way. For the single site map we choose an antisymmetric tent map (cf. Fig. 4). But for the coupling we resort to a symbolic coupling which only takes the sign of the coordinates of nearby lattice points

into account. Thus, we are able to employ the analytical techniques described in the previous sections. To be definite consider a simple square lattice with periodic boundary conditions and let $\nu=(\nu_1,\nu_2)$ label the lattice sites. As before $\underline{x}=(x^{(\nu)})$ and $\underline{\sigma}=(\sigma^{(\nu)})$ denote the actual and the symbolic state of the system, respectively, where $\sigma^{(\nu)}=\mathrm{sgn}(x^{(\nu)})$. For the map acting on the lattice site ν we take the form depicted in Fig. 4

$$[T(\underline{x})]^{(\nu)}=\begin{cases}-1+2(1-x^{(\nu)})/(1-a_+) & \text{if} \quad a_+<x^{(\nu)}<1\\ x^{(\nu)}/a_+ & \text{if} \quad 0<x^{(\nu)}<a_+\\ x^{(\nu)}/a_- & \text{if} \quad -a_-<x^{(\nu)}<0\\ 1-2(1+x^{(\nu)})/(1-a_-) & \text{if} \quad -1<x^{(\nu)}<-a_-\end{cases}. \tag{21}$$

The spatial coupling is introduced by letting the parameters $a_\pm$ of the map depend on the sum of the nearest neighbor symbols

$$\Sigma_{\underline{\sigma}}^{(\nu)}=\sigma^{(\nu_1+1,\nu_2)}+\sigma^{(\nu_1-1,\nu_2)}+\sigma^{(\nu_1,\nu_2+1)}+\sigma^{(\nu_1,\nu_2-1)}. \tag{22}$$

For our particular model we choose

$$a_{\sigma^{(\nu)}}[\Sigma_{\underline{\sigma}}^{(\nu)}]=\tanh(J_0+J_{nn}\sigma^{(\nu)}\Sigma_{\underline{\sigma}}^{(\nu)}). \tag{23}$$

The spatial coupling in the map lattice is thus mediated by the constant J_{nn} which, in fact, has to obey the constraint $|J_{nn}|<J_0/4$ in order to keep the map lattice (21) well defined. We will see later on that the particular choice (23) ensures detailed balance of the corresponding probabilistic cellular automaton.

There is, of course, no guarantee that the coupled map lattice just introduced has something in common with the original Miller-Huse model. However, one has to keep in mind that the diffusive coupling usually employed in numerical studies of coupled map lattices has no real justification as well. The symbolic coupling used here has the advantage of being accessible by analytical means as one is essentially dealing with a dynamical system admitting a skew product structure.

The probabilistic cellular automaton can be easily derived from Eqs. (21) and (23) using the formal approach of Appendix A. In fact, a heuristic inspection of the single site map indicates that a "spin flip" at lattice site ν, $\sigma^{(\nu)}\to-\sigma^{(\nu)}$, will occur with probability $(1-a_{\sigma^{(\nu)}}[\Sigma_{\underline{\sigma}}^{(\nu)}])/2$. Thus, the rate for the process $\tau^{(\nu)}\to\sigma^{(\nu)}$ is given by

$$\frac{1+\sigma^{(\nu)}\tau^{(\nu)}a_{\tau^{(\nu)}}[\Sigma_{\underline{\tau}}^{(\nu)}]}{2}=\frac{\exp[\sigma^{(\nu)}(J_0\tau^{(\nu)}+J_{nn}\Sigma_{\underline{\tau}}^{(\nu)})]}{2\cosh(J_0\tau^{(\nu)}+J_{nn}\Sigma_{\underline{\tau}}^{(\nu)})}, \tag{24}$$

where we have used Eq. (23). Thus, we infer the transition rates of the master equation [cf. Eq. (7)] to be given by the expression

$$W(\underline{\sigma};\underline{\tau})=\frac{\exp\left(\sum_\nu\sigma^{(\nu)}(J_0\tau^{(\nu)}+J_{nn}\Sigma_{\underline{\tau}}^{(\nu)})\right)}{\prod_\nu 2\cosh(J_0+J_{nn}\tau^{(\nu)}\Sigma_{\underline{\tau}}^{(\nu)})}. \tag{25}$$

Of course, the same expression is obtained when the piecewise linear density is used for evaluating the Frobenius-Perron equation of the coupled map lattice.

The master equation obeys detailed balance since the effective field related with the transition probabilities (25) is symmetric with respect to space inversion. In fact

$$\frac{W(\underline{\sigma};\underline{\tau})}{W(\underline{\tau};\underline{\sigma})}=\frac{\prod_\nu 2\cosh(J_0+J_{nn}\sigma^{(\nu)}\Sigma_{\underline{\sigma}}^{(\nu)})}{\prod_\nu 2\cosh(J_0+J_{nn}\tau^{(\nu)}\Sigma_{\underline{\tau}}^{(\nu)})}=\frac{p_*(\underline{\sigma})}{p_*(\underline{\tau})} \tag{26}$$

and the two-dimensional spin Hamiltonian associated with the stationary density is given by

$$-\ln p_*(\underline{\sigma})=-\sum_\nu\ln\cosh(J_0+J_{nn}\sigma^{(\nu)}\Sigma_{\underline{\sigma}}^{(\nu)})-\ln(2/Z). \tag{27}$$

The two-dimensional Hamiltonian (27) produces phase transitions [29]. If, for instance, one considers the limit $J_0\gg1$ then, apart from exponentially small corrections, the logarithm and the hyperbolic function in Eq. (27) cancel and we end up with a nearest neighbor coupled Ising model. A ferromagnetic phase transition appears at $J_{nn}=J_c=\ln(\sqrt{2}+1)/4=0.2203,\ldots,$. Thus, spatial correlations of the coupled map lattice (21) decay exponentially for $0\leqslant J_{nn}<J_c$, while the up down symmetry of large lattices is spontaneously broken for strong coupling $J_{nn}>J_c$. The qualitative behavior can be easily confirmed by numerical simulations (cf. Fig. 5). Even for rather small values of J_0 the prediction of the critical coupling seems to be quite accurate and an Ising-type phase transition is found when the time evolution of the total magnetization $m_n=\Sigma_\nu\sigma_n^{(\nu)}/L^2$ and the state of the symbol lattice are observed.

There is a quite simple explanation why the invariant density of the coupled map lattice approaches the canonical distribution of the two-dimensional Ising model in the limit $J_0\gg1$. In this limit the parameter (23) is close to 1 so that transitions in the sign of the coordinate, i.e., spin flips, hap-

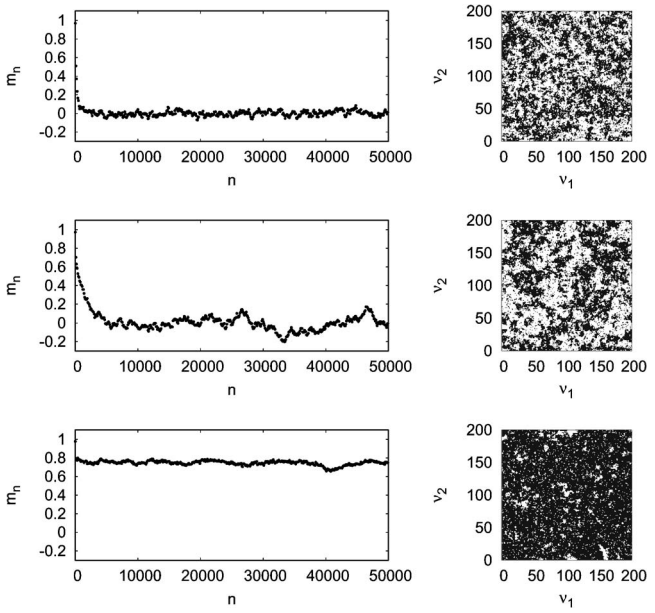

FIG. 5. Numerical simulation of the coupled map lattices (21) and (23) for $J_0=1.25$ on a square lattice of size 200×200 with periodic boundary conditions. Time dependence of the magnetization $m_n=\Sigma_\nu\sigma_n^{(\nu)}/L^2$ (left) and the final state of the symbol lattice at $n=50000$ (right) when a ferromagnetic initial state has been used. Top, subcritical coupling $J_{nn}=0.20$; middle, "critical" coupling $J_{nn}=0.22$; bottom, supercritical coupling $J_{nn}=0.24$.

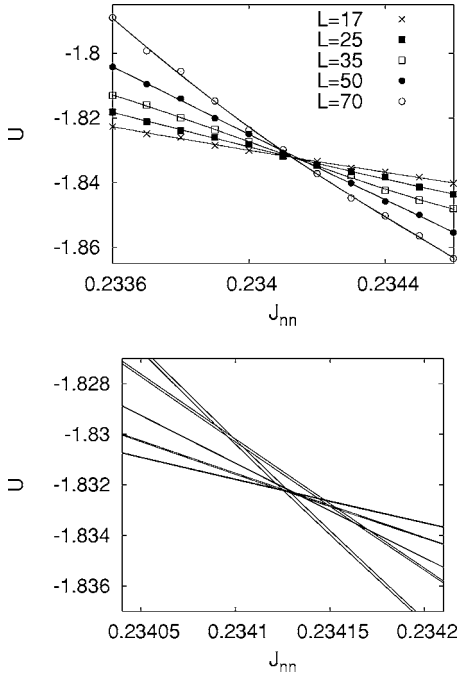

FIG. 6. Top: Numerical computation of the Binder cumulant (28) for the coupled map lattices (21) and (23) with $J_0=1.25$ and different system sizes. For each value of the system size L the lines display a cubic and quartic least square fit to the data points. The two lines cannot be distinguished at the scale of the graph. Bottom: Graph of the Binder cumulants on a smaller scale. Cubic and quartic fits to the data points can now be distinguished.

pen rarely (cf. Fig. 4). Thus, even in a large lattice there are almost no simultaneous changes of sign. The symbolic dynamics is equivalent to a kinetic Ising model with random updates, and the canonical distribution of a nearest neighbor coupled Ising model is obtained for the stationary state.

Of course, one can easily analyze the Hamiltonian determined by Eq. (27) for smaller values of J_0 as well using some standard algebra. To keep the presentation self-contained Appendix C contains some details. Apart from nearest neighbor and next nearest neighbor interactions the Hamiltonian contains as well two types of four spin interactions (cf. [26] for a closely related result). These interactions are short ranged and mainly ferromagnetic. Thus general wisdom about renormalization suggests that the model falls within the Ising universality class. Although an analytical proof is not obvious such an assertion can be tested easily by numerical means.

V. FINITE SIZE SCALING ANALYSIS

Critical behavior and the corresponding universality class can be quantified by various critical exponents. Actually, for the accurate numerical determination of such exponents one may resort to procedures very well established in the context of equilibrium and nonequilibrium physics [24]. Such concepts have been applied to coupled map lattices [22] and probabilistic cellular automata [30] as well. Three critical exponents which are quite easy to evaluate are related with the power law behavior of the magnetization, the susceptibility, and the spatial correlation length, $M\sim(J_{nn}-J_c)^\beta$, $\chi\sim|J_{nn}-J_c|^{-\gamma}$, $\xi\sim|J_{nn}-J_c|^{-\nu}$, in the thermodynamic limit $L\to\infty$. To obtain reliable values for such exponents one has to resort to a finite size scaling approach [24]. The key quantities to be computed are moments $\langle m^n\rangle$ of the magnetization $m=\Sigma_\nu\sigma^{(\nu)}/L^2$ where $\langle\,\rangle$ denotes an ensemble average, i.e., a long time average in the case of dynamical systems. By observing the dependence of such moments on the system size L and on the coupling strength J_{nn} one is able to determine accurate estimates for the critical point J_c and for the critical exponents β, γ, and ν.

To begin with one needs an estimate for the critical coupling. Such an estimate can be obtained by computing the so-called Binder cumulant

$$U(L,J_{nn})=-3+\frac{\langle m^4\rangle}{\langle m^2\rangle^2} \tag{28}$$

in dependence on L and J_{nn}. The finite size scaling hypothesis guarantees that the Binder cumulant depends on the two variables only through the combination $(J_{nn}-J_c)L^{1/\nu}$. Thus, for different values of the system size L the graphs of the Binder cumulant considered as a function of the coupling strength J_{nn} all intersect in a common point which determines the critical coupling J_c. Figure 6 displays data for the coupled map lattice (21) obtained for various system sizes. Throughout our simulations we fix the value of the parameter $J_0=1.25$. The ensemble averages have been computed from a time series of length $n=10^9$ and in each case 5% of the simulation time has been discarded to allow for the decay of

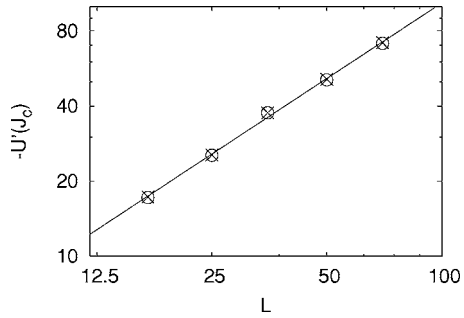

FIG. 7. Derivative of the Binder cumulant at the critical coupling strength in dependence of the system size. Data points have been obtained from the cubic (×) and quartic (○) fit to the data displayed in Fig. 6. The straight line shows a least square fit.

the transient dynamics. To a very good degree the graphs of the Binder cumulant intersect at a critical value of the coupling strength. To improve the accuracy of the estimate Fig. 6 shows the behavior on a smaller scale as well. Fits to the data points yield an intersection region and we produce a conservative estimate for the critical coupling, $J_c = 0.234\ 13 \pm 0.000\ 03$.

To obtain the exponent ν one may consider the derivative of the Binder cumulant with respect to the coupling J_{nn} at the critical coupling strength. Actually applying the finite size scaling hypothesis we have

$$\left.\frac{\partial U}{\partial J_{nn}}\right|_{J_{nn}=J_c} \sim L^{1/\nu}. \tag{29}$$

We estimate the derivative by computing the slope of the cubic and the quartic fit at the critical coupling strength. The data for the slope in dependence on the system size are shown in Fig. 7. The order of the fit plays apparently a minor role. The double logarithmic plot yields a confirmation of the power law scaling and the least square fit yields for the exponent the estimate $\nu = 0.994 \pm 0.015$.

The exponent β can be determined essentially from the scaling of the finite size magnetization at the critical coupling strength, $J_{nn}=J_c$. The finite size scaling hypothesis yields

$$\langle |m| \rangle \sim L^{-\beta/\nu}. \tag{30}$$

The data displayed in Fig. 8 confirm such a power law behavior with an exponent $\beta/\nu = 0.1245 \pm 0.0005$. The third exponent can be obtained from the scaling of the finite size susceptibility at the critical point

$$\chi = L^2(\langle m^2 \rangle - \langle |m| \rangle^2) \sim L^{\gamma/\nu}. \tag{31}$$

The data displayed in Fig. 8 again confirm a power law with an estimate for the exponent $\gamma/\nu = 1.748 \pm 0.003$.

Within the statistical error bars the measured exponents agree with the Ising universality class, $\nu=1$, $\beta=\frac{1}{8}$, and $\gamma=\frac{7}{4}$, as expected. The current analysis shows what accuracy can be achieved when the critical behavior of coupled map lattices is at stake. In particular, the accurate determination of the critical coupling seems to be crucial as otherwise the values of the exponents may be corrupted. In the present case

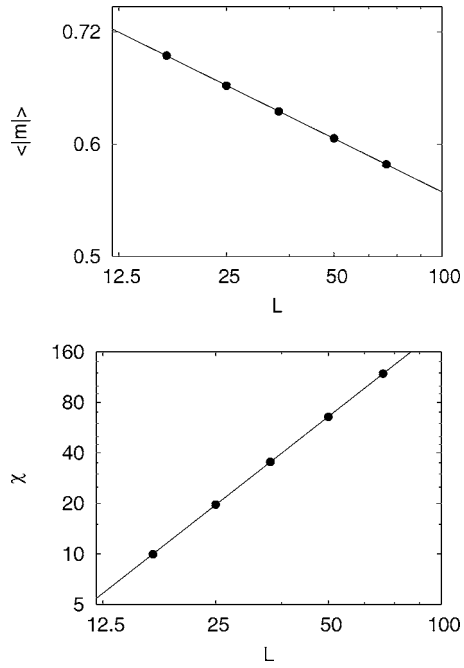

FIG. 8. Top: Dependence of the first moment of $m=\Sigma_\nu \sigma^{(\nu)}/L^2$ at $J_c = 0.234\ 13$ on the system size L. The straight line shows a least square fit with slope $= -0.1245 \pm 0.0005$. Bottom: Dependence of the finite size susceptibility (31) at J_c on the system size L. The straight line indicates a least square fit with slope 1.748 ± 0.003.

the analysis of the Binder cumulant does not display a systematic drift of the intersections with the system size (cf. Fig. 6) as it was sometimes reported in the analysis of coupled map lattices [22,30]. Error bars for ν are apparently quite large as this exponent was based on the derivative of a polynomial fit. The other two ratios of exponents are more accurate as they are directly evaluated from the scaling behavior of appropriate moments. Overall, the results are far from surprising since the underlying equilibrium Hamiltonian has short range and predominantly ferromagnetic interactions.

VI. DISCUSSION

Piecewise linear coupled map lattices with a coupling mediated by the symbolic coordinate can be analyzed by analytical means. The dynamics can be described in terms of probabilistic cellular automata if some Markov-like conditions for the partition are satisfied. One may object against such particular types of spatial couplings. First of all the skew product structure between the coordinates and the symbols is slightly artificial although it is the essential ingredient for the analytical approach. Second, the usually employed diffusive coupling is, in general, not covered by such a scheme. One should, however, keep in mind that there is no real justification for such a coupling although it is employed in the vast majority of numerical approaches. Despite these shortcomings one should mention that within the restricted class of dynamical systems considered here one gets some insight into the statistical properties of spatially extended dynamical systems. In that respect such special coupled map lattices may be of the same relevance like piecewise linear

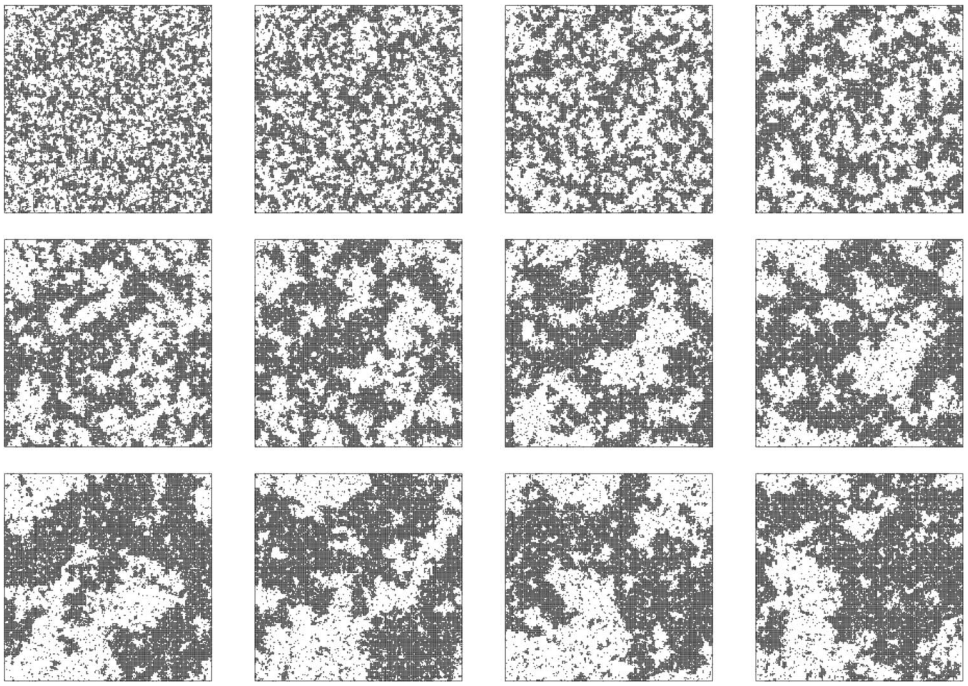

FIG. 9. Temporal evolution of the symbolic state of the Miller-Huse-like coupled map lattice (21) on a 200×200 lattice with periodic boundary conditions at the critical coupling, $J_0=1.25$, $J_{nn}=J_c=0.234\,13$. Plots are shown at times (left to right and top to bottom) $n=25$, 50, 100, 200,…, 12 800, and 25 600. A random initial condition, i.e., the "high temperature" state, has been used.

Markov maps in the context of low-dimensional chaotic systems. Last but not least one should mention that the coupling through the symbolic coordinate is able to cover the famous diffusive coupling as well if piecewise linear dynamics on repelling sets is considered.

Spatially one-dimensional coupled map lattices are able to display phase transitions, i.e., qualitative changes of the dynamics which are entirely related to the limit of large system size, since the symbolic dynamics yields spin models on two-dimensional symbol lattices. However, if one requires the dynamics to act on an attracting set then constraints are imposed on the corresponding spin Hamiltonian which may remove the possibility of phase transitions. Thus, coupled map lattices on repelling sets allow for a larger variety. The occurrence of phase transitions is more likely in such a setup although such a behavior cannot be reproduced by straightforward numerical simulations. Furthermore, the occurrence of the disorder condition for the symbolic dynamics of d-dimensional coupled map lattices with attracting sets might explain why such systems show critical behavior according to a universality class of a d-dimensional spin system, like the Miller-Huse model, despite a space time symbolic dynamics that yields a $d+1$-dimensional spin Hamiltonian.

Detailed balance is required as well to compute analytical expressions for the invariant density and for the correlation functions of coupled maps and of probabilistic cellular automata. Whenever the transition rates of the latter models are products of quantities which involve only spins from a local neighborhood then the condition of detailed balance necessarily yields a stationary distribution which is generated by a spin Hamiltonian with short range interactions. Thus, spatial correlations decay exponentially when one-dimensional models are considered and phase transitions are unlikely to occur in such a setup. Detailed balance or the violation of detailed balance seems to be a vital ingredient when phase transitions in one-dimensional models are considered. Even for local transition rates the corresponding stationary distribution and the effective Hamiltonian may contain long range interactions causing phase transitions when detailed balance is violated.

Phase transitions for expanding map lattices and probabilistic cellular automata without absorbing states are of course easily possible for spatially two-dimensional coupled systems. The Miller-Huse-like model introduced in Sec. IV constitutes a simple example. Detailed balance is obeyed and a Hamiltonian with short range predominately ferromagnetic interaction results. General wisdom of the renormalization group theory predicts critical behavior according to the Ising universality class and such a behavior has been confirmed by the computation of some critical exponents. Thus, contrary to previous conjectures simultaneous updating is here not the essential argument. Detailed balance plays the much more important role. We have entirely focused on some static critical exponents. One may consider as well dynamical critical features. I do not intend to discuss the corresponding scaling behavior in detail but the temporal evolution of a disordered initial state displays coarsening phenomena at the critical point (cf. Fig. 9). Thus, the observations are in accordance with Ising universality and detailed balance seems to be a vital ingredient for such a behavior. One might expect that minor violations of detailed balance do not change the universality class so that the features are somehow stable with respect to variations of the model [31]. However, substantial violations of detailed balance, as one might expect to occur

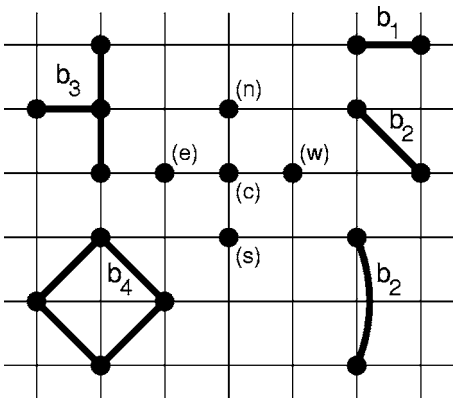

FIG. 10. Labeling of the "central" lattice site (c) and its four nearest neighbors (e), (n), (w), and (s). Diagrammatic view of the two spin and four spin interactions appearing in the local energy contribution (C2), apart from rotations.

for the original Miller-Huse model, may change the critical behavior and may be responsible for the deviation from Ising universality which has been reported previously [22]. Certainly, further investigations are needed and the analysis of probabilistic cellular automata might be of help to solve such a puzzle.

The numerical finite size scaling procedure which has been performed in Sec. V produces, as expected, critical exponents in accordance with the Ising universality class. The analysis gives a hint of which size of errors one has to expect when critical behavior of coupled map lattices is analyzed by such an approach. In particular, the accurate determination of the critical point seems to be crucial as otherwise the numerical estimates for the critical exponents may be corrupted. Let me mention that in the current case no systematic drift of the Binder cumulant with the system size has occurred as it was reported in some related investigations [22,30]. Whether such a drift is related with the violation of detailed balance cannot be solved at the current stage. Nevertheless, there seems to be substantial unsolved problems in connection with the statistical mechanics of coupled map lattices which deserve to be discussed.

APPENDIX A: FROM COUPLED MAP LATTICES TO PROBABILISTIC CELLULAR AUTOMATA

Let $\rho_n(\underline{x})$ denote the probability distribution to be in state $\underline{x}$ at time n. The time dependence of such a distribution is governed by the celebrated Frobenius-Perron equation (cf. e.g., [32])

$$\rho_{n+1}(\underline{x}) = \int \prod_{\nu} \delta\{x^{(\nu)} - f[y^{(\nu)}; \tau^{(\nu+1)} = \mathrm{sgn}(y^{(\nu+1)})]\}\rho_n(\underline{y})d\underline{y} \tag{A1}$$

when we consider the dynamics according to Eq. (1). To simplify Eq. (A1) consider the hypercubes of the generating partition, i.e., $U_{\underline{\sigma}} = U_{\sigma^{(0)}} \times U_{\sigma^{(1)}} \times \cdots \times U_{\sigma^{(L-1)}}$ and denote the characteristic function of this cube by

$$\chi_{\underline{\sigma}}(\underline{x}) = \begin{cases} 1 & \text{if } \underline{x} \in U_{\underline{\sigma}} \\ 0 & \text{if } \underline{x} \notin U_{\underline{\sigma}}. \end{cases} \tag{A2}$$

By a straightforward calculation we will show that piecewise constant densities, i.e.,

$$\rho_n(\underline{x}) = \sum_{\underline{\tau}} \chi_{\underline{\tau}}(\underline{x}) p_n(\underline{\tau}) \tag{A3}$$

yield a solution of Eq. (A1). Namely we have

$$\begin{aligned}
\rho_{n+1}(\underline{x}) &= \int \prod_{\nu} \delta\{x^{(\nu)} - f[y^{(\nu)}; \tau^{(\nu+1)} = \mathrm{sgn}(y^{(\nu+1)})]\}\rho_n(\underline{y})d\underline{y} \\
&= \sum_{\underline{\tau}} \int_{U_{\underline{\tau}}} \prod_{\nu} \delta[x^{(\nu)} - f(y^{(\nu)}; \tau^{(\nu+1)})]d\underline{y}\, p_n(\underline{\tau}) \\
&= \sum_{\underline{\tau}} \sum_{\underline{\sigma}} \chi_{\underline{\sigma}}(\underline{x}) \int_{U_{\underline{\tau}}} \prod_{\nu} \delta[x^{(\nu)} - f(y^{(\nu)}; \tau^{(\nu+1)})]d\underline{y}\, p_n(\underline{\tau}) \\
&= \sum_{\underline{\sigma}} \sum_{\underline{\tau}} \chi_{\underline{\sigma}}(\underline{x}) \prod_{\nu} \int_{U_{\tau^{(\nu)}}} \int \delta[x^{(\nu)} \\
&\quad - f(y^{(\nu)}; \tau^{(\nu+1)})]dy^{(\nu)}\Big|_{x^{(\nu)} \in U_{\sigma^{(\nu)}}} p_n(\underline{\tau}) \\
&= \sum_{\underline{\sigma}} \chi_{\underline{\sigma}}(\underline{x}) \sum_{\underline{\tau}} \prod_{\nu} \frac{1}{\gamma_{\tau^{(\nu)}\sigma^{(\nu)}}[\tau^{(\nu+1)}]} p_n(\underline{\tau}).
\end{aligned} \tag{A4}$$

Thus, piecewise constant densities are preserved when iterating the dynamics according to Eq. (A1). The weights $p_n(\underline{\tau})$ then obey the master equation (7) with transition rates given by Eq. (8).

APPENDIX B: STATIONARY DENSITIES AND DETAILED BALANCE

The stationary density of Eq. (7) is just determined by the time-independent master equation which in view of the normalization of the transition matrix can be written as

$$0 = \sum_{\underline{\tau}} [W_f(\underline{\sigma}; \underline{\tau}) p_*(\underline{\tau}) - W_f(\underline{\tau}; \underline{\sigma}) p_*(\underline{\sigma})]. \tag{B1}$$

Although the determination of the stationary density is usually a difficult task it becomes almost trivial when detailed balance is satisfied, i.e., the individual terms of the sum in Eq. (B1) vanish separately. Such probabilistic cellular automata are often referred as being reversible and numerous investigations of such models can be found in the literature (cf. e.g., [29,31,33]). When the transition probabilities are written in terms of an effective field, like Eq. (8), then it is quite well established that the condition of detailed balance, i.e., the Kolmogorov criterion [34], requires the field to be symmetric with respect to lattice inversion [15,26]. Such a condition is not met by the model given in terms of W_f. But as we have seen in Sec. II the model is still easily solvable. Actually, the model obeys a slight generalization of detailed

balance as pointed out recently [27]. The condition of stationarity, Eq. (B1), can be ensured as well if the contribution $W_f(\underline{\sigma};\underline{\tau})p_*(\underline{\tau})$ is balanced by a term $W_f(\underline{\tilde{\tau}};\underline{\sigma})p_*(\underline{\sigma})$, which does not necessarily involve the same spin state $\underline{\tau}$, as long as the mapping $\underline{\tau}\to\underline{\tilde{\tau}}$ introduced by this constraint is one-to-one. Actually, for the model W_f it is quite straightforward to establish such a mapping which depends on the spin state $\underline{\sigma}$. If we choose

$$\tilde{\tau}^{(\nu)} = \tau^{(\nu-1)}\sigma^{(\nu)}\sigma^{(\nu+1)} \tag{B2}$$

then a simple calculation based on Eqs. (8) and (9) yields

$$\begin{aligned}\frac{W_f(\underline{\sigma};\underline{\tau})}{W_f(\underline{\tilde{\tau}};\underline{\sigma})} &= \frac{\exp\left(\sum_\nu \sigma^{(\nu)}(\lambda\tau^{(\nu)}+\mu\tau^{(\nu+1)})\right)\prod_\nu 2\cosh(\lambda\sigma^{(\nu)}+\mu\sigma^{(\nu+1)})}{\exp\left(\sum_\nu \tilde{\tau}^{(\nu)}(\lambda\sigma^{(\nu)}+\mu\sigma^{(\nu+1)})\right)\prod_\nu 2\cosh(\lambda\tau^{(\nu)}+\mu\tau^{(\nu+1)})} \\ &= \frac{\exp\left(\sum_\nu \tau^{(\nu)}(\lambda\sigma^{(\nu)}+\mu\sigma^{(\nu-1)})\right)\prod_\nu 2\cosh(\lambda\sigma^{(\nu)}+\mu\sigma^{(\nu+1)})}{\exp\left(\sum_\nu \tilde{\tau}^{(\nu)}(\lambda\sigma^{(\nu)}+\mu\sigma^{(\nu+1)})\right)\prod_\nu 2\cosh(\lambda\tau^{(\nu)}+\mu\tau^{(\nu+1)})} \\ &= \frac{\exp\left(\sum_\nu \tau^{(\nu)}(\lambda\sigma^{(\nu)}+\mu\sigma^{(\nu-1)})\right)\prod_\nu 2\cosh(\lambda\sigma^{(\nu)}+\mu\sigma^{(\nu+1)})}{\exp\left(\sum_\nu \tau^{(\nu+1)}(\lambda\sigma^{(\nu+1)}+\mu\sigma^{(\nu)})\right)\prod_\nu 2\cosh(\lambda\tau^{(\nu)}+\mu\tau^{(\nu+1)})} = \frac{\prod_\nu 2\cosh(\lambda\sigma^{(\nu)}+\mu\sigma^{(\nu+1)})}{\prod_\nu 2\cosh(\lambda\tau^{(\nu)}+\mu\tau^{(\nu+1)})} = \frac{p_*(\underline{\sigma})}{p_*(\underline{\tau})},\end{aligned} \tag{B3}$$

where the transformation (B2) has been employed as well. Thus, the stationary density obeys a slight generalization of detailed balance

$$W_f(\underline{\sigma};\underline{\tau})p_*(\underline{\tau}) = W_f(\underline{\tilde{\tau}};\underline{\sigma})p_*(\underline{\sigma}). \tag{B4}$$

Probabilistic cellular automata of such a type have been called "quasi-Hamiltonian automata" [15]. Similar considerations are well known as well in the context of Fokker-Planck equations [35] when one takes properties of the variables with respect to time reversal and the corresponding reversible probability current into account. Thus, the model defined by W_f can still be considered to be a kind of reversible probabilistic cellular automaton when trivial currents are accounted for.

APPENDIX C: INTERACTION POTENTIALS

The determination of the interaction terms of the Hamiltonian (27) in terms of pair and multispin interactions is a standard procedure. Here we recall the essential steps on an elementary level to keep the presentation self-contained. Consider the contribution with index ν to the sum in Eq. (27). Denote the central spin at lattice site ν by the label (c) and its four nearest neighbors by (e) (east), (n) (north), (w) (west), and (s) (south) (cf. Fig. 10). If $\Sigma=\sigma^{(e)}+\sigma^{(n)}+\sigma^{(w)}+\sigma^{(s)}$ denotes the total spin of the nearest neighbors then the contribution to the Hamiltonian (27) reads

$$\begin{aligned}-\ln\cosh(J_0+J_{nn}\sigma^{(c)}\Sigma) = a_0 + a_1\sigma^{(c)}\Sigma + a_2\Sigma^2 + a_3\sigma^{(c)}\Sigma^3 \\ + a_4\Sigma^4,\end{aligned} \tag{C1}$$

where the right-hand side follows by series expansion taking into account that $\sigma^{(c)}\Sigma$ takes even integer values only, $\sigma^{(c)}\Sigma=0,\pm2,\pm4$. If we evaluate the powers we obtain the expansion

$$\begin{aligned}-\ln\cosh(J_0+J_{nn}\sigma^{(c)}\Sigma) = b_0 &+ b_1\sigma^{(c)}(\sigma^{(e)}+\sigma^{(n)}+\sigma^{(w)}+\sigma^{(s)}) \\ &+ b_2(\sigma^{(n)}\sigma^{(w)}+\sigma^{(n)}\sigma^{(e)}+\sigma^{(s)}\sigma^{(w)} \\ &+ \sigma^{(s)}\sigma^{(e)}+\sigma^{(n)}\sigma^{(s)}+\sigma^{(w)}\sigma^{(e)}) \\ &+ b_3\sigma^{(c)}(\sigma^{(n)}\sigma^{(w)}\sigma^{(s)}+\sigma^{(n)}\sigma^{(e)}\sigma^{(s)} \\ &+ \sigma^{(n)}\sigma^{(e)}\sigma^{(w)}+\sigma^{(s)}\sigma^{(e)}\sigma^{(w)}) \\ &+ b_4\sigma^{(n)}\sigma^{(e)}\sigma^{(w)}\sigma^{(s)},\end{aligned} \tag{C2}$$

where the expansion coefficients b_k still need to be expressed in terms of the original parameters J_0 and J_{nn}. Nevertheless the algebra shows so far that the Hamiltonian displays a nearest neighbor pair interaction involving the central spin, two next nearest neighbor pair interactions which do not involve the central spin, and two types of four spin interactions which do and do not involve the central spin, respectively (cf. Fig. 10).

The evaluation of the interaction coefficients b_k is now completely straightforward. By considering $\sigma^{(c)}=\pm1$ and adding and subtracting the corresponding equations, the system (C2) can be decoupled partially

$$\begin{aligned}-\tfrac{1}{2}[\ln\cosh(J_0+J_{nn}\Sigma)+\ln\cosh(J_0-J_{nn}\Sigma)] \\ = b_0 + b_2(\sigma^{(n)}\sigma^{(w)}+\sigma^{(n)}\sigma^{(e)}+\sigma^{(s)}\sigma^{(w)}+\sigma^{(s)}\sigma^{(e)}+\sigma^{(n)}\sigma^{(s)} \\ + \sigma^{(w)}\sigma^{(e)}) + b_4\sigma^{(n)}\sigma^{(e)}\sigma^{(w)}\sigma^{(s)} \\ -\tfrac{1}{2}[\ln\cosh(J_0+J_{nn}\Sigma)-\ln\cosh(J_0-J_{nn}\Sigma)]\end{aligned}$$

$$= b_1(\sigma^{(e)} + \sigma^{(n)} + \sigma^{(w)} + \sigma^{(s)}) + b_3(\sigma^{(n)}\sigma^{(w)}\sigma^{(s)} + \sigma^{(n)}\sigma^{(e)}\sigma^{(s)} + \sigma^{(s)}\sigma^{(e)}\sigma^{(w)} + \sigma^{(n)}\sigma^{(e)}\sigma^{(w)}). \quad \text{(C3)}$$

Considering nearest neighbor spin configurations with $\Sigma=0$, 2, 4 we obtain from Eq. (C3)

$$\begin{aligned} -\ln\cosh J_0 &= b_0 - 2b_2 + b_4 \\ &\quad - \tfrac{1}{2}[\ln\cosh(J_0 + 2J_{nn}) + \ln\cosh(J_0 - 2J_{nn})] \\ &= b_0 - b_4 \\ &\quad - \tfrac{1}{2}[\ln\cosh(J_0 + 2J_{nn}) - \ln\cosh(J_0 - 2J_{nn})] \\ &= 2b_1 - 2b_3 \\ &\quad - \tfrac{1}{2}[\ln\cosh(J_0 + 4J_{nn}) + \ln\cosh(J_0 - 4J_{nn})] \\ &= b_0 + 6b_2 + b_4 \\ &\quad - \tfrac{1}{2}[\ln\cosh(J_0 + 4J_{nn}) - \ln\cosh(J_0 - 4J_{nn})] \\ &= 4b_1 + 4b_3. \end{aligned} \quad \text{(C4)}$$

Equation (C4) is now solved easily and the final result reads

$$b_0 = -\ln\cosh(J_0) - \tfrac{1}{2}\Delta_2(2J_{nn}) - \tfrac{1}{8}\Delta_2(4J_{nn}) \simeq -\ln\cosh(J_0),$$

$$b_1 = -\tfrac{1}{8}\Delta_1(2J_{nn}) - \tfrac{1}{16}\Delta_1(4J_{nn}) \simeq -\tfrac{1}{2}\tanh(J_0)J_{nn},$$

$$b_2 = -\tfrac{1}{8}\Delta_2(4J_{nn}) \simeq -\frac{1}{\cosh^2(J_0)}J_{nn}^2,$$

$$b_3 = \tfrac{1}{8}\Delta_1(2J_{nn}) - \tfrac{1}{16}\Delta_1(4J_{nn}) \simeq -\frac{\tanh(J_0)}{\cosh^2(J_0)}J_{nn}^3,$$

$$b_4 = -\tfrac{1}{8}\Delta_2(4J_{nn}) + \tfrac{1}{2}\Delta_2(2J_{nn}) \simeq \frac{2\sinh^2(J_0) - 1}{\cosh^4(J_0)}J_{nn}^4, \quad \text{(C5)}$$

where

$$\Delta_1(x) = \ln\cosh(J_0 + x) - \ln\cosh(J_0 - x),$$

$$\Delta_2(x) = \tfrac{1}{2}[\ln\cosh(J_0 + x) + \ln\cosh(J_0 - x) - 2\ln\cosh(J_0)], \quad \text{(C6)}$$

abbreviate discrete derivatives of first and second order. The asymptotic expressions in Eq. (C5) state the leading order with respect to the coupling constant J_{nn}.

In the limit $J_0 \gg 1$ all interactions but b_1 become exponentially small and the Hamiltonian reduces to a nearest neighbor coupled Ising model. The interactions are predominantly ferromagnetic for $J_{nn} > 0$. In the case $J_0 = 0$ the model reduces to the Hamiltonian already investigated in [26].

[1] J. P. Eckmann and D. Ruelle, Rev. Mod. Phys. **57**, 1115 (1985).
[2] C. Robinson, *Dynamical Systems: Stability, Symbolic Dynamics, and Chaos* (CRC Press, Boca Raton, FL, 1995).
[3] H. G. Schuster, *Deterministic Chaos* (VCH, Weinheim, 1995).
[4] E. Ott, *Chaos in Dynamical Systems* (Cambridge University Press, Cambridge, 1993).
[5] M. C. Cross and P. C. Hohenberg, Rev. Mod. Phys. **65**, 851 (1993).
[6] S. H. Strogatz, Physica D **143**, 1 (2000).
[7] K. Kaneko, Physica D **34**, 1 (1989).
[8] K. Kaneko, *Theory and Applications of Coupled Map Lattices* (Wiley, Chichester, 1993).
[9] L. A. Bunimovich and Y. G. Sinai, Nonlinearity **1**, 491 (1988).
[10] J. Bricmont and A. Kupiainen, Nonlinearity **8**, 379 (1995).
[11] T. Fischer and H. H. Rugh, Ergod. Theory Dyn. Syst. **20**, 109 (2000).
[12] *Dynamics of Coupled Map Lattices and of Related Spatially Extended Systems*, edited by J. R. Chazottes and B. Fernandez, Lecture Notes in Physics Vol. 671 (Springer, Berlin, 2005).
[13] D. Ruelle, *Thermodynamic Formalism* (Addison-Wesley, Reading, 1978).
[14] G. Gielis and R. S. MacKay, Nonlinearity **13**, 867 (2000).
[15] A. Georges and P. L. Doussal, J. Stat. Phys. **54**, 1011 (1989).
[16] J. L. Lebowitz, C. Maes, and E. R. Speer, J. Stat. Phys. **59**, 117 (1990).
[17] J. Miller and D. A. Huse, Phys. Rev. E **48**, 2528 (1993).
[18] A. Politi, R. Livi, G.-L. Oppo, and R. Kapral, Europhys. Lett. **22**, 571 (1993).
[19] M. Blank and L. Bunimovich, Nonlinearity **16**, 387 (2003).
[20] W. Just, J. Stat. Phys. **105**, 133 (2001).
[21] R. S. MacKay, in *Dynamics of Coupled Map Lattices and of Related Spatially Extended Systems* (Ref. [12]), p. 65.
[22] P. Marcq, H. Chaté, and P. Manneville, Phys. Rev. E **55**, 2606 (1997).
[23] R. J. Glauber, J. Math. Phys. **4**, 294 (1963).
[24] K. Binder, *Monte Carlo Simulation in Statistical Physics: An Introduction* (Springer, Berlin, 1992).
[25] W. Just and F. Schmüser, in *Dynamics of Coupled Map Lattices and of Related Spatially Extended Systems* (Ref. [12]), p. 33.
[26] E. N. M. Cirillo, F. R. Nardi, and A. D. Polosa, Phys. Rev. E **64**, 057103 (2001).
[27] F. Schmüser and W. Just, J. Stat. Phys. **105**, 525 (2001).
[28] T. Schultz, D. Mattis, and E. Lieb, Rev. Mod. Phys. **36**, 856 (1964).
[29] P. D. Pra, P.-Y. Louis, and S. Roelly, ESAIM: Probab. Stat. **6**, 89 (2002).
[30] D. Makowiec, Phys. Rev. E **60**, 3787 (1999).
[31] G. Grinstein, C. Jayaprakash, and Y. He, Phys. Rev. Lett. **55**, 2527 (1985).
[32] A. Lasota and M. C. Mackey, *Chaos, Fractals, and Noise: Stochastic Aspects of Dynamics* (Springer, New York, 1994).
[33] S. Bigelis, E. N. M. Cirillo, J. L. Lebowitz, and E. R. Speer, Phys. Rev. E **59**, 3935 (1999).
[34] F. P. Kelly, *Reversibility and Stochastic Networks* (Wiley, Chichester, 1979).
[35] H. Risken, *The Fokker-Planck Equation: Methods of Solution and Applications* (Springer, Berlin, 1989).